A&A 495, 707–719 (2009)
DOI: 10.1051/0004-6361:200810997

Astronomy & Astrophysics

WINGS-SPE
Spectroscopy in the WIde-field Nearby Galaxy-cluster Survey⋆

A. Cava[1,2,3], D. Bettoni[1], B. M. Poggianti[1], W. J. Couch[4], M. Moles[5], J. Varela[1], A. Biviano[6], M. D'Onofrio[7], A. Dressler[8], G. Fasano[1], J. Fritz[1], P. Kjærgaard[9], M. Ramella[6], and T. Valentinuzzi[7]

[1] INAF – Osservatorio Astronomico di Padova, Vicolo dell'Osservatorio 5, 3512 Padova, Italy
[2] Università degli Studi di Milano, Dipartimento di Fisica, via Celoria 16, 20133 Milano, Italy
[3] Instituto de Astrofísica de Canarias, C/Vía Lactea s/n, 38205 La Laguna, Tenerife, Spain
e-mail: acava@iac.es
[4] Centre for Astrophysics and Supercomputing, Swinburne University of Technology, Hawthorn VIC 3122, Australia
[5] Instituto de Astrofísica de Andalucía (C.S.I.C.) Apartado 3004, 18080 Granada, Spain
[6] INAF – Osservatorio Astronomico di Trieste, via Tiepolo 11, 34143 Trieste, Italy
[7] Università degli Studi di Padova, Dipartimento di Astronomia, Vicolo Osservatorio 3, 35122 Padova, Italy
[8] Observatories of the Carnegie Institution of Washington, Pasadena, CA 91101, USA
[9] Copenhagen University Observatory. The Niels Bohr Insitute for Astronomy Physics and Geophysics, Juliane Maries Vej 30, 2100 Copenhagen, Denmark

Received 19 September 2008 / Accepted 5 December 2008

ABSTRACT

Aims. We present the results from a comprehensive spectroscopic survey of the WINGS (WIde-field Nearby Galaxy-cluster Survey) clusters, a program called WINGS-SPE. The WINGS-SPE sample consists of 48 clusters, 22 of which are in the southern sky and 26 in the north. The main goals of this spectroscopic survey are: (1) to study the dynamics and kinematics of the WINGS clusters and their constituent galaxies, (2) to explore the link between the spectral properties and the morphological evolution in different density environments and across a wide range of cluster X-ray luminosities and optical properties.
Methods. Using multi-object fiber-fed spectrographs, we observed our sample of WINGS cluster galaxies at an intermediate resolution of 6–9 Å and, using a cross-correlation technique, we measured redshifts with a mean accuracy of ∼45 km s^{-1}.
Results. We present redshift measurements for 6137 galaxies and their first analyses. Details of the spectroscopic observations are reported. The WINGS-SPE has ∼30% overlap with previously published data sets, allowing us both to perform a complete comparison with the literature and to extend the catalogs.
Conclusions. Using our redshifts, we calculate the velocity dispersion for all the clusters in the WINGS-SPE sample. We almost triple the number of member galaxies known in each cluster with respect to previous works. We also investigate the X-ray luminosity vs. velocity dispersion relation for our WINGS-SPE clusters, and find it to be consistent with the form $L_x \propto \sigma_v^4$.

Key words. galaxies: clusters: general – galaxies: distances and redshifts

1. Introduction

Rich clusters of galaxies have long been recognized as valuable tools in which to study cosmology and galaxy formation. They are the most massive virialized objects in the universe and, as such, provide excellent laboratories for studying the influence of environment on galaxy formation and evolution, as manifested by the morphology-density relation (Dressler 1980; Dressler et al. 1997; Fasano et al. 2000; Postman et al. 2005). The identification of the properties and content of clusters of galaxies is able to clarify their cosmic evolution since they can be detected at large distances. However clusters of galaxies are now recognized not to be simple relaxed structures; rather, they are evolving via merging processes in a hierarchical fashion from poor groups to rich clusters. In fact in the cluster outskirts, galaxies are still falling in for the first time, so it is possible also to explore environmental effects over a wide dynamic range in density.

Clusters contain large populations of galaxies at a common distance, which can be used to derive redshift-independent relative distance estimates (Dressler et al. 1987). This allows the study of deviations from pure Hubble flow, i.e., the peculiar velocity field, and hence the dark matter distribution in the local universe (e.g., Lynden-Bell et al. 1988; see also Dekel 1994; Strauss & Willick 1995, for reviews). Cluster velocity dispersions provide a measure of cluster mass (Fisher et al. 1998; Tran et al. 1999; Borgani et al. 1999a; Lubin et al. 2002). The measurement of cluster velocity dispersions should be made using statistics insensitive to galaxy redshift outliers and the shape of the velocity distribution. However, the uncertainties in these studies are large, and there remains the possibility of systematic errors due to the heterogeneity of the spectroscopic data sets available for nearby clusters ($z < 0.1$). In recent years, a systematic investigation of a large sample of nearby clusters has become possible due to the advent of CCD mosaics and high multiplex multi-object fiber-fed spectrographs,

⋆ Table 4, containing the complete redshift catalog, is only available in electronic form at the CDS via anonymous ftp to cdsarc.u-strasbg.fr (130.79.128.5) or via http://cdsweb.u-strasbg.fr/cgi-bin/qcat?J/A+A/495/707

allowing photometric and spectroscopic observations over large solid angles (Smith et al. 2004; Fasano et al. 2006).

In the last few years, large redshift surveys such as the 2dF Galaxy Redshift Survey (hereafter 2dFGRS; De Propris et al. 2002) and especially the Sloan Digital Sky Survey (SDSS, Goto et al. 2002; Bahcall et al. 2003; Miller et al. 2005) have been the primary source for the compilation of data on nearby clusters of galaxies. However, both these surveys have their limitations. The 2dFGRS is only a spectroscopic survey while the SDSS, being a large area survey, is not deep enough to study the fainter end of the luminosity function. More recently, the NOAO Fundamental Plane Survey (Smith et al. 2004) started to address these shortcomings.

The need for accurate redshift measurements has also become evident from the great progress that has been made in recent years in the observations of the signatures of cluster merging processes. The presence of substructure, which is indicative of a cluster in an early phase of the process of dynamical relaxation or of secondary infall of clumps into already virialized clusters, occurs in a large percentage of clusters (Dressler & Shectman 1988; West & Bothun 1990; Rhee et al. 1991; Bird 1994; Escalera et al. 1994; West et al. 1995; Girardi et al. 1997; Solanes et al. 1999; Biviano et al. 2002 ; Burgett et al. 2004; Flin & Krywult 2006). Studying cluster substructure therefore allow us to investigate the process by which clusters form. In addition, it also enables us to better understand the mechanisms affecting galaxy evolution in clusters, which can be accelerated by the effects of a cluster-subcluster collision. An interesting result has been produced by our recent study (Ramella et al. 2007) in which we point out that the fraction of clusters with sub-clusters in the WINGS sample (73%) is higher than in most previous studies. In addition, in a subsequent paper of the WINGS-SPE series (Cava et al. 2009, in prep.) a more detailed analysis of the sub-clustering in the WINGS sample will be included, exploiting and comparing different 2D and 3D approaches.

In this paper we present redshifts for galaxies in 48 clusters belonging to the Wide-field Imaging Nearby Galaxy-cluster Survey (WINGS) sample. In addition, we present cluster velocity dispersion measurements derived from our redshift data. These clusters comprise an almost complete X-ray selected sample of galaxy clusters at $z = 0.04$–0.07 (see Fasano et al. 2006, for details of the survey).

The main goal of the WINGS-SPE spectroscopic follow-up program is to supply a complete and uniform set of spectroscopic data such as redshift (present paper), line indices, and line widths useful to investigate the dynamics of the clusters and derive star formation histories, star formation rates (Fritz et al. 2007; Fritz et al. 2009, in prep.), and other structural and physical properties of cluster galaxies. These new data will shed more light on the link between the evolution of star formation and galaxy morphology, as well as the dependence on the characteristics of the cluster and where the galaxies are located within the cluster. Furthermore, the availability of data on low redshift clusters can be used as a present-day reference for studies of distant clusters (see e.g. Poggianti et al. 2006).

This paper is organized as follows: In Sect. 2 we give general information on the WINGS-SPE objectives and working strategy; in Sect. 3 we present the spectroscopic observations and describe the reduction processes; in Sect. 4 redshift measurements and catalogs are presented, while in Sect. 5 we check the data quality performing a comparison with data in the literature. Finally we draw our conclusions in Sect. 6.

2. Survey strategy

WINGS clusters (see Fasano et al. 2006 for details) have been selected from three X-ray flux limited samples compiled from ROSAT All-Sky Survey data: the ROSAT Brightest Cluster Sample (Ebeling et al. 1998, BCS), and its extension (Ebeling et al. 2000, eBCS) in the northern hemisphere and the X-ray-Brightest Abell-type Cluster sample (Ebeling et al. 1996, XBACs) in the southern hemisphere.

The global sample contains 77 clusters (36 in the northern hemisphere and 41 in the south) over a broad range of richness, Bautz-Morgan class and X-ray luminosities. Our aim was to obtain spectroscopic data for the whole sample. However, bad weather conditions (we lost ~25% of our observing time, mainly during the northern sample observations) prevented us from reaching this goal. For this reason the final WINGS-SPE sample contains 48 (of the 77) clusters, 22 of which are in the southern sky and 26 are in the northern sky. This sample was extracted from the main sample giving the highest observing priority to clusters with few (less than 20) or no redshifts available from the literature. For example, clusters A0085, A0548b, and Abell 3558, which have large databases of available redshifts, had a lower priority.

The target selection was based on the available WINGS optical B, V photometry (Varela et al. 2009) and the aim of the target selection strategy was to maximize the chances of observing galaxies at the cluster redshift without biasing the cluster sample. The main criteria for selecting spectroscopic targets were similar for the northern and southern samples, the only difference being the fibre size. In both cases, we selected galaxies with a V magnitude within the fiber aperture of $V < 21.5$ (although in a very few cases galaxies at fainter magnitudes have been observed) and with a color within a 5 kpc aperture of $(B - V)_{5\ \mathrm{kpc}} \lesssim 1.4$. These loose selection limits were applied so as to avoid any bias in the observed morphological type, as is the case of a selection based on the CM relation only (which selects just red, early type galaxies). The exact cut in color was varied slightly from cluster to cluster in order to account for the redshift variation and to optimize the observational setup. Our total apparent magnitude limit ($V \sim 20$) is 1.5 to 2.0 mag deeper than the 2dFRS and Sloan surveys, and this is, in general, reflected in a higher mean number of member galaxies detected per cluster.

In Table 1, we list the main properties of the clusters in the WINGS-SPE sample. The different columns indicate: (1) cluster name, (2–3) coordinates of the image field center at epoch $J2000$ [right ascension (2) in hours, minutes and seconds and declination (3) in degrees, arcminutes, arcseconds], (4) number of redshifts, which is equal to the number of entries in the spectroscopic catalog for that cluster, (5) mean cluster redshift, (6) number of member galaxies (used to compute mean redshift and velocity dispersion as explained in Sect. 4), (7) cluster velocity dispersion computed from the WINGS-SPE data, (8) cluster velocity dispersion available from the literature, (9) reference for the literature velocity dispersion, (10) logarithm of the X-ray luminosity in the 0.1–2.4 keV ROSAT RASS bandpass (from Ebeling et al. 1996), (11) virial radius in Mpc, (12) aperture in units of R_{200}. For completeness, we also list in Table 2 the main properties of the 29 clusters not observed but for which literature data exist. The different columns here indicate: (1) cluster name, (2–3) coordinates of the image field center at epoch $J2000$ [right ascension (2) in hours, minutes and seconds and declination (3) in degrees, arcminutes, arcseconds], (4) cluster mean redshift, (5) number of member galaxies, (6) cluster velocity dispersion, (7) reference for the data reported in Cols. (4–6),

Table 1. The WINGS-SPE cluster sample: global properties.

Cluster	RA (J2000)	Dec (J2000)	N_{gal}	z	N_z	σ_W km s^{-1}	σ_L km s^{-1}	Refs.	$\log(L_X)$ 10^{44} erg s^{-1}	R_{200} Mpc	Ap R_{200}
A0119	00:56:21.37	–01:15:46.5	248	0.0444	158	$866^{\pm55}$	740	st99	44.51	2.10	0.6
A0151	01:08:52.35	–15:25:00.9	269	0.0532	92	$762^{\pm57}$	669	st99	44.00	1.84	0.9
A0160	01:12:51.40	+15:30:53.8	80	0.0438	40	$784^{\pm111}$	572	st99	43.58	1.90	0.6
A0193	01:25:07.35	+08:41:35.9	62	0.0485	40	$761^{\pm86}$	756	st99	44.19	1.84	0.6
A0376	02:45:48.53	+36:51:35.5	88	0.0476	66	$949^{\pm90}$	519	st99	44.14	2.29	0.6
A0500	04:38:54.97	–22:05:55.3	140	0.0678	89	$729^{\pm55}$	...	...	44.15	1.75	0.9
A0671	08:28:29.28	+30:25:00.6	35	0.0507	20	$956^{\pm130}$	1043	st99	43.95	2.31	0.5
A0754	09:08:50.08	–09:38:11.8	158	0.0547	132	$961^{\pm57}$	931	st99	44.90	2.32	0.6
A0957x	10:13:57.33	–00:54:54.4	128	0.0451	65	$704^{\pm52}$	659	st99	43.89	1.70	0.7
A0970	10:17:34.30	–10:42:01.5	185	0.0591	117	$771^{\pm42}$	...	...	44.18	1.85	0.8
A1069	10:39:54.29	-08:36:39.8	112	0.0653	40	$690^{\pm68}$	1120	st99	43.98	1.65	0.9
A1291	11:32:04.46	+56:01:26.2	85	0.0509	27	$413^{\pm65}$	720	ag07	43.64	1.0	1.3
A1631a	12:52:49.84	–15:26:17.1	227	0.0461	126	$717^{\pm38}$	702	st99	43.86	1.73	0.9
A1644	12:57:14.77	–17:21:12.6	266	0.0467	176	$1051^{\pm58}$	945	st99	44.55	2.54	0.5
A1795	13:49:00.52	+26:35:06.8	91	0.0633	53	$658^{\pm81}$	887	g96	45.05	1.58	1.0
A1831	13:59:10.19	+27:59:27.9	66	0.0634	17	$444^{\pm68}$	316	st94	44.28	1.07	1.5
A1983	14:52:44.00	+16:44:45.8	94	0.0447	45	$522^{\pm36}$	498	st94	43.67	1.26	0.9
A1991	14:54:30.22	+18:37:51.2	50	0.0584	35	$625^{\pm73}$	721	st99	44.13	1.50	0.9
A2107	15:39:47.91	+21:46:20.6	41	0.0410	36	$626^{\pm83}$	625	g96	44.04	1.52	0.6
A2124	15:44:59.33	+36:03:39.9	46	0.0666	30	$596^{\pm58}$	826	ag07	44.13	1.43	1.0
A2169	16:14:06.63	+49:07:30.6	63	0.0578	37	$524^{\pm60}$	521	ag07	43.65	1.26	1.1
A2382	21:52:01.87	–15:38:53.1	247	0.0641	152	$835^{\pm58}$	...	...	43.96	2.00	0.8
A2399	21:57:32.55	–07:47:40.4	242	0.0578	125	$716^{\pm46}$	530	st99	44.00	1.72	0.9
A2415	22:05:25.01	–05:35:23.1	199	0.0575	98	$698^{\pm52}$	...	...	44.23	1.68	1.1
A2457	22:35:45.20	+01:28:33.3	81	0.0584	56	$648^{\pm51}$	316	st99	44.16	1.56	1.0
A2572a	23:18:23.58	+18:44:24.7	26	0.0390	21	$546^{\pm103}$	676	st99	44.01	1.33	0.8
A2589	23:24:00.52	+16:49:29.0	47	0.0419	35	$830^{\pm98}$	819	st99	44.27	2.01	0.4
A2593	23:24:31.01	+14:38:29.3	86	0.0417	53	$627^{\pm67}$	763	st99	44.06	1.52	0.7
A2622	23:34:53.81	+27:25:35.5	71	0.0610	38	$732^{\pm68}$	942	st99	44.03	1.76	0.6
A2626	23:36:31.00	+21:09:36.3	70	0.0548	36	$679^{\pm60}$	696	st99	44.29	1.64	0.7
A3128	03:30:34.63	–52:33:12.2	297	0.0600	207	$900^{\pm38}$	802	st99	44.33	2.16	0.8
A3158	03:42:39.64	–53:37:50.1	278	0.0593	177	$1090^{\pm53}$	976	st99	44.73	2.62	0.6
A3266	04:31:11.92	–61:24:22.7	264	0.0593	225	$1389^{\pm66}$	1085	st99	44.79	3.34	0.4
A3376	06:00:43.57	–40:02:59.5	144	0.0461	92	$814^{\pm56}$	641	st99	44.39	1.97	0.6
A3395	06:27:31.09	–54:23:57.8	191	0.0500	125	$755^{\pm49}$	1090	st99	44.45	1.82	0.7
A3490	11:45:18.58	–34:26:40.0	218	0.0688	83	$660^{\pm47}$	...	...	44.24	1.58	1.1
A3497	12:00:03.53	–31:23:42.4	165	0.0680	82	$724^{\pm48}$	...	...	44.16	1.73	1.3
A3556	13:24:06.23	–31:39:37.8	175	0.0479	114	$584^{\pm45}$	643	st99	43.97	1.41	0.8
A3560	13:31:50.50	–33:13:25.4	191	0.0489	118	$717^{\pm43}$	1123	st99	44.12	1.73	0.9
A3809	21:46:51.76	–43:52:54.7	195	0.0627	104	$561^{\pm40}$	499	st99	44.35	1.35	1.1
IIZW108	21:13:56.00	+02:33:56.0	32	0.0483	27	$549^{\pm42}$	...	...	44.34	1.33	0.6
MKW3s	15:21:50.00	+07:42:32.0	66	0.0444	32	$539^{\pm37}$	612	g96	44.43	1.31	0.7
RX0058	00:58:22.30	+26:52:03.7	31	0.0484	22	$696^{\pm119}$	...	...	43.64	1.68	0.7
RX1022	10:22:07.30	+38:30:55.0	44	0.0548	25	$582^{\pm91}$	591	ag07	43.54	1.40	1.0
RX1740	17:40:32.30	+35:38:57.0	32	0.0441	20	$540^{\pm66}$	...	...	43.70	1.31	0.8
Z2844	10:02:37.09	+32:41:16.7	54	0.0503	33	$529^{\pm84}$	...	...	43.76	1.28	0.7
Z8338	18:11:26.75	+49:49:47.4	86	0.0494	53	$686^{\pm71}$	...	...	43.90	1.66	0.7
Z8852	23:10:31.85	+07:34:17.7	71	0.0408	53	$696^{\pm67}$	...	...	43.97	1.69	0.5

Refs: (st94) Struble & Ftaclas (1994); (g96) Girardi et al. (1996); (maz96) Mazure et al. (1996); (wu98) Wu et al. (1998); (st99) Struble & Rood (1999); (FPS04) Smith et al. (2004); (ag07) Aguerri et al. (2007). Columns: (1) cluster name, (2–3) coordinates of the image field center at epoch 2000 (right ascension (2) in hours, minutes and seconds and declination (3) in degrees, arcminutes, arcseconds), (4) number of redshift determinations which is equal to the number of entries in the spectroscopic catalog for that cluster, (5) cluster mean redshift, (6) number of member galaxies (used to compute mean redshift and velocity dispersion as explained in the text), (7) cluster velocity dispersion computed from WINGS data, (8) cluster velocity dispersion from literature, (9) reference for the literature velocity dispersion, (10) logarithm of the X-ray luminosity in the 0.1–2.4 keV ROSAT RASS bandpass (from Ebeling et al. 1996), (11) virial radius in Mpc, (12) aperture in units of R_{200}.

Table 2. Global properties of the remaining 29 clusters of the WINGS sample.

Cluster	RA (J2000)	Dec (J2000)	z	N_z	σ_L km s^{-1}	Refs.	log (L_X) 10^{44} erg s^{-1}
A0085	00:41:37.81	–09:20:33.2	0.0521	273	979	ag07	44.92
A0133	01:02:38.97	–21:57:15.4	0.0603	7	623	st99	44.55
A0147	01:08:10.44	+02:09:59.9	0.0447	11	387	st99	43.73
A0168	01:15:09.80	+00:14:50.6	0.0448	106	578	ag07	44.04
A0311	02:09:10.34	+19:43:10.4	0.0657	1	...	wu98	43.91
A0548b	05:47:01.74	-25:36:58.8	0.0441	323	842	st99	43.48
A0602	07:53:19.02	+29:21:10.5	0.0621	78	834	ag07	44.05
A0780	09:18:30.36	–12:15:40.1	0.0565	34	...	FPS04	44.82
A1668	13:03:51.41	+19:15:55.1	0.0634	15	654	st99	44.20
A1736	13:26:52.16	–27:06:33.5	0.0461	109	918	st99	44.37
A2149	16:01:38.10	+53:52:42.9	0.0675	20	459	ag07	43.92
A2256	17:03:43.53	+78:43:02.6	0.0581	116	1376	st99	44.85
A2271	17:17:17.53	+78:01:00.0	0.0584	10	460	st99	43.80
A2657	23:44:51.00	+09:08:39.6	0.0400	31	829	st99	44.20
A2665	23:50:45.44	+06:06:41.2	0.0562	2	...	st99	44.28
A2717	00:02:59.40	–36:02:05.5	0.0498	56	512	st99	44.00
A2734	00:11:20.13	–28:52:18.5	0.0624	80	628	st99	44.41
A3164	03:45:49.70	–57:02:43.9	0.0611	3	991	st99	44.17
A3528a	12:54:31.28	–29:22:21.6	0.0535	28	969	maz96	44.12
A3528b	12:54:08.64	–28:50:32.5	0.0535	6	...	FPS04	44.30
A3530	12:55:36.88	–30:21:14.4	0.0544	...	391	wu98	43.94
A3532	12:57:19.17	–30:22:12.7	0.0555	44	742	st99	44.45
A3558	13:27:54.77	–31:29:31.8	0.0477	341	977	st99	44.80
A3562	13:33:31.81	–31:40:22.5	0.0502	114	1048	st99	44.52
A3667	20:12:30.09	–56:48:59.5	0.0530	162	1059	st99	44.94
A3716	20:51:16.71	–52:41:43.5	0.0448	111	733	st99	44.00
A3880	22:27:49.53	–30:34:40.0	0.0570	22	855	st99	44.27
A4059	23:56:40.70	–34:40:17.7	0.0480	45	628	FPS04	44.49
Z1261	07:16:42.60	+53:24:28.0	0.0644	...	...	wu98	43.91

Refs: (st94) Struble & Ftaclas (1994); (g96) Girardi et al. (1996); (maz96) Mazure et al. (1996); (wu98) Wu et al. (1998); (st99) Struble & Rood (1999); (FPS04) Smith et al. (2004); (ag07) Aguerri et al. (2007).
Columns: (1) cluster name, (2–3) coordinates of the image field center at epoch 2000 (right ascension (2) in hours, minutes and seconds and declination (3) in degrees, arcminutes, arcseconds), (4) cluster mean redshift, (5) number of member galaxies, (6) cluster velocity dispersion (7) reference for the data reported in columns (4-6), (8) logarithm of the X-ray luminosity in the 0.1–2.4 keV ROSAT RASS bandpass (from Ebeling et al. 1996).

(8) logarithm of the X-ray luminosity in the 0.1–2.4 keV ROSAT RASS bandpass (from Ebeling et al. 1996).

3. Spectroscopic data

3.1. Observations and data reduction

The spectroscopic observations were obtained over the course of 6 observing runs (22 nights) at the 4.2 m William Herschel Telescope (WHT) using the AF2/WYFFOS multifiber spectrograph and 3 observing runs (11 nights) at the 3.9 m Anglo Australian Telescope (AAT) using the 2dF multifiber spectrograph. The spectroscopic runs are summarized in Table 3.

AF2/WYFFOS is the multi-object, wide-field, fiber spectrograph working at the 4.2 m William Herschel Telescope (WHT) on La Palma. AF2/WYFFOS can allocate up to 150 fibres, each of 1.6 arcsec diameter. We typically allocated 60–70 fibers to objects in a given configuration, and on average, 15–20 sky fibers. For runs 1–5, we used the AF2/WYFFOS Long Camera with the TEK6 1024 × 1024 CCD with pixel size of 24 μ. In combination with the 600B grism that was used, this yielded a spectral resolution of ∼6 Å *FWHM*, depending on the location on the CCD. For run 6 we again used the 600B grism, but with the 2-chip

Table 3. The WINGS-SPE observing runs.

Run	Telescope	Date	$\lambda FWHM$ (Å)
1	WYFFOS@WHT	Aug./Sept. 2002	6
2	WYFFOS@WHT	April 2003	6
3	WYFFOS@WHT	June 2003	6
4	WYFFOS@WHT	March 2004	6
5	WYFFOS@WHT	June 2004	6
6	WYFFOS@WHT	Oct. 2004	3.2
7	2dF@AAT	Jan. 2003	9
8	2dF@AAT	Sept. 2003	9
9	2dF@AAT	March 2004	9

EEV 4300 × 4300 mosaic with 13.5 μ pixels. With a 2 × 2 binning of the CCD pixels, this gave a spectral resolution of ∼3 Å *FWHM*. The spectra were centred at a wavelength of 5100 Å and covered the range ∼3800–7000Å. Hence they covered many interesting spectral features ranging from Ca H&K in the blue to NaD in the red. The galaxies were divided into different configurations, depending on their luminosities. Two configurations were executed for each cluster: one bright (V < 20.5 inside the

1.6″ aperture) and one faint ($20.5 < V < 21.5$ inside the 1.6″ aperture), with total exposure times of 1 h for the bright sample and 2 h for the faint one. He/Argon lamp exposures for wavelength calibration and offset sky exposures for fibre throughput calibration were also obtained. We also observed spectroscopic flux standards, Lick standards, and radial velocity standards during twilight. The reduction of these multi-fiber spectra was performed using the *dofiber* IRAF package.

The multiple exposures in each pointing were combined, with cosmic rays being rejected in the process. Twilight sky flats or combined object frames were used to define the apertures and trace the spectra on the CCD. The median offset sky exposures were then used to calculate the throughput for each fiber, and to normalize all of the sky fibres. The arc spectra were extracted and matched with standard arc lines to determine the dispersion solution using a polynomial fit. These fits yielded a typical rms scatter of 0.05 Å. Finally, the object spectra were extracted, normalized, and wavelength calibrated. A master sky spectrum was derived for each exposure by combining the spectra from 10–30 individual sky fibers. The fibers do not all have identical throughput, and in some runs the differences could not be adequately determined from the calibration flat-field pectra obtained. In order to perform accurate sky subtraction, we scaled the master sky spectrum based on the flux in the bright 5577 Å line to minimize residuals in each galaxy spectrum. At the end of this procedure the sky subtraction accuracy was quite good, ranging between 1–3% (defined as the rms of the normalized sky fibres about the master sky spectrum).

For the southern sample, we used the Two-degree Field (2dF) multifiber spectrograph on the AAT (runs 7–9). This instrument can observe up to 400 objects simultaneously over a two degree field of view. The detectors were 1024 × 1024 24 μm pixel Tektronix CCDs, which in combination with the 300B grating yielded a resolution of 9 Å and a wavelength range of 3600–8000 Å. The fiber diameter is 2″. The galaxies were again divided into two different configurations in order to observe multiple sets of galaxies brighter and fainter than $V = 19.5$ in the fibre. For each cluster we were able in this way to observe ∼150–200 target galaxies. The integration times were generally 1 and 2 h for the bright and faint configurations, respectively. For each field we first took a multi-fiber flat-field exposure using the quartz lamp in the calibration unit. This flat-field is used to trace the positions of the fibres on the CCD image, to fit the spatial profile of each fiber as a function of wavelength, and to apply a 1-dimensional pixel-to-pixel flat-field correction to the extracted spectra. Exposures of helium and copper-argon arc lamps were taken for wavelength calibration. The data were reduced at the telescope using the 2dF data reduction (*2dfdr*) pipeline software, a full description of which is given by Taylor et al. (1996, see also http://www.aao.gov.au/2df). The main steps in the process are as follows: bias subtraction and flat fielding, mapping of the spectra with background subtraction and finally wavelength calibration. However the standard sky subtraction does not work well for all the spectra; in general systematic residuals are evident where skylines have been subtracted, in particular for the faint ones. For this reason we re-extracted from each configuration the spectra from individual sky fibers, derived a master sky spectrum and subtracted this spectrum from the original wavelength calibrated spectra. At the end of this procedure the sky subtraction accuracy was quite good, ranging between 1–3% (as in the case of the northern sample). Sample spectra of galaxies with different luminosities in the bright and faint samples are shown in Fig. 1 for the northern sample and in Fig. 2 for the southern one.

3.2. Flux calibration

Absolute flux calibration can never be performed with fibers, since we are limited by the fixed fiber diameter. Following the recipes of the 2dFGRS survey (Lewis et al. 2002), the following procedure was adopted to perform a relative flux calibration. First we applied the response function available from the 2dF web site (Lewis et al. 2002). This response curve can be applied, on average, to give an approximate relative flux calibration for the 2dF spectra. However, the results for individual spectra will vary considerably due to sky subtraction and efficiency variations over each plate. In order to obtain an optimal flux calibration correction we decided to perform a comparison with SDSS spectra for a set of galaxies in common to the two samples. From this comparison we derived a mean correction curve that was applied to all the spectra of the southern sample.

For the northern sample, spectrophotometric standard stars were observed in order to be able to flux calibrate the data. These star spectra were reduced and wavelength calibrated with the same "dofiber" package. Typically, one star was observed at the start of the night and another one at the end of the night and at least in two different fibers. For the nights for which a full sample of standard stars in different fibers was available, we used the average sensitivity function derived using all stars observed that night. Unfortunately, due to bad weather conditions there were nights when each flux standard was observed through one fiber only. Having verified that the curve from fiber to fiber for the different standard stars all agreed well (less than 10% difference), the data taken in those nights lacking a full sample of standard stars were calibrated using the average sensitivity function of all the other nights. As a final step, all the spectra were corrected for atmospheric extinction using the extinction curves published for Siding Spring and La Palma Observatories, respectively.

4. Redshifts measurements

In this work, radial velocities were measured using procedures based on the Fourier cross-correlation method (Tonry & Davis 1981), as implemented in the *xcsao* task in the RVSAO package. RVSAO (Kurtz & Mink 1998) is an IRAF add-on package developed at the Smithsonian Astrophysical Observatory Telescope Data Center to obtain radial velocities from spectra using cross-correlation and emission line fitting techniques.

We note that the redshifts obtained via *xcsao* are unreliable in cases where the observed spectrum departs markedly from that of the template star (taken from Jacoby et al. 1984), or when the galaxy spectrum contains strong emission lines. To determine redshifts with greater robustness, a set of template galaxy spectra was also used. As template galaxy spectra we used a sample of spectra with high S/N extracted from our data as well as synthetic emission line spectra generated using the task "RVSAO/linespec". This task reads a list of positions of emission lines and creates a spectrum with Gaussian lines of the indicated half-widths at the indicated positions, writing a one-dimensional IRAF file. The galaxy templates include both pure absorption and emission-dominated spectra. All the spectra were inspected by eye to verify the redshift measurements and to ensure that the best matching template was chosen. Finally we checked the spectra for possible residual shifts due to systematic errors in the wavelength calibration. In order to correct for residual shifts we cross-correlated each spectrum (before sky

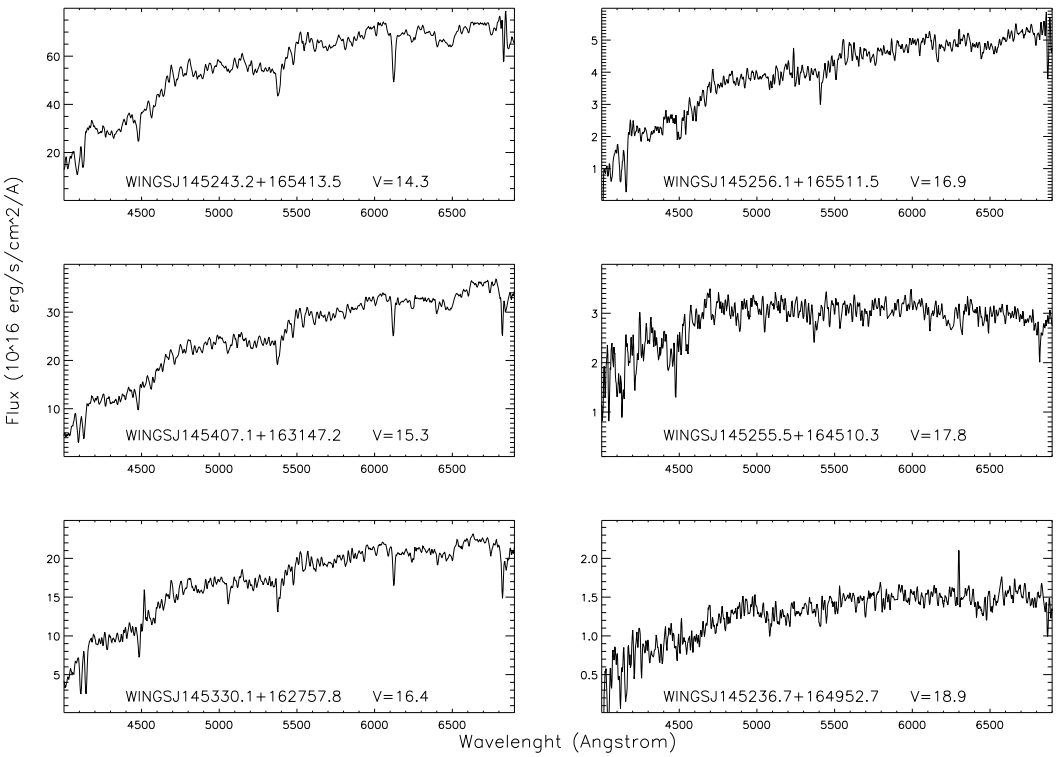

Fig. 1. Sample spectra for the northern sample observed with WYFFOS spectrograph at WHT. Spectra of bright (*left*) and faint (*right*) galaxies are shown for the cluster A1983. The object IDs and V-band magnitudes are given in each panel.

subtraction) with a template sky spectrum. The final redshift has been corrected for the measured displacements of the skylines with respect to the zero-point. After this correction, each radial velocity measurement was corrected to the heliocentric velocity. We chose to limit the spectral range used in the cross-correlation to the interval 3800 Å $\leq \lambda \leq$ 6800 Å, because in the blue region the spectra are very noisy outside of this range, and in the red region the spectra are dominated by the strong telluric bands.

Summarizing, the procedure followed to measure the redshifts was as follows:

- determination of the redshift of the galaxies using a semi-automated method;
- determination of the displacement of the skylines with respect to the zero-point and correction for this;
- spectra with uncertain redshifts flagged and checked again manually to ensure the best reliability.

The redshift distribution of the whole spectroscopic sample is presented in Fig. 3. An example catalogue can be seen in Table 4. The different columns are:
Column (1) gives the object name, Col. (2) gives the right ascension (J2000), and Col. (3) gives the declination (J2000), Col. (4) gives the redshift, in km s^{-1}, and Col. (5) the redshift error in km s^{-1}, Col. (6) gives the correlation factor r defined as:

$$r = \frac{h}{\sqrt{2}\sigma_a} \tag{1}$$

which is the ratio between the height, h, of the main peak to the mean height, σ_a, of the secondary peaks in the Fourier cross-correlation function (Tonry & Davies 1981). Assuming sinusoidal noise, with the half-width of the sinusoid equal to the half-width of the correlation peak this factor can be related to the measurement error (Kurtz & Mink 1998) as:

$$\delta = \frac{3}{8}\frac{w}{1+r} \tag{2}$$

where w is the $FWHM$ of the correlation peak. Only spectra achieving a correlation factor higher than 2 have been considered reliable after the visual check; the mean r is equal to 8 and 83% of the redshift determinations have a correlation factor greater than 4 ensuring that the measurements are highly reliable.

Column (7) gives the membership flag; a value of 1 indicates the galaxy is a cluster member, and a value of 0 indicates it is either a background or foreground galaxy. Cluster membership is defined on the basis of the galaxy redshift being within $\pm 3\sigma$ from $z_{\rm cl}$ (see Sect. 6).

Column (8) indicates the cluster field to which the galaxy belongs. The complete version of Table 4 is available in electronic format only.

5. Data quality

5.1. External comparisons

Previous spectroscopic surveys have yielded redshift measurements for a substantial number of galaxies in common with the WINGS-SPE sample. Here we employ these data to test the reliability of our data. We use data from the NASA/IPAC Extragalactic Database (NED) to perform our comparison with the aim of extending our catalogs and exploiting the entire dataset (WINGS+literature) in the kinematical and dynamical analysis. In particular, we intend to use these data to study in detail the properties of clusters and substructures in the WINGS sample (see Ramella et al. 2007, for the study of substructures

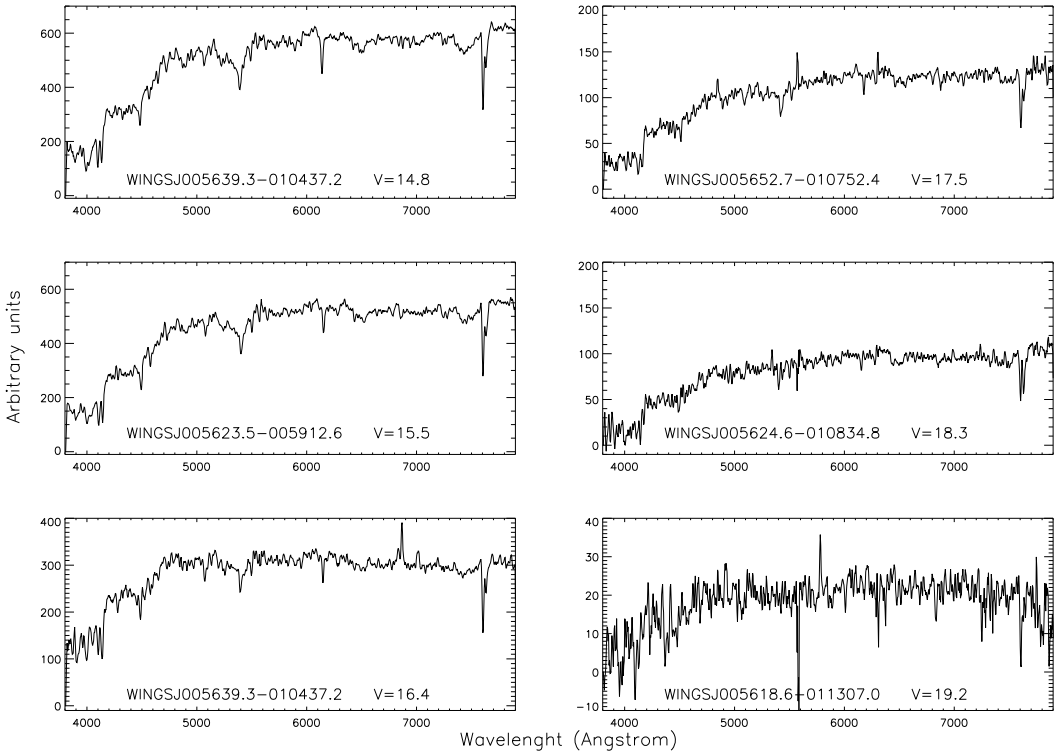

Fig. 2. Example of spectra for the southern sample observed with 2dF spectrograph at AAT. Spectra of bright (*left*) and faint (*right*) galaxies are shown for the cluster A0119. The object IDs and *V*-band magnitudes are given in each panel.

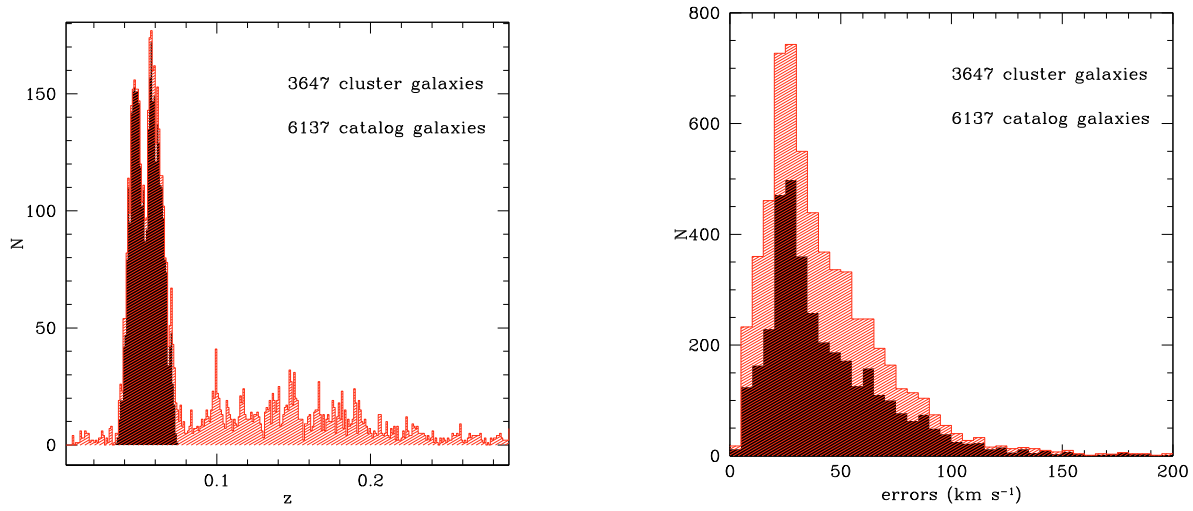

Fig. 3. Distribution of redshifts (*left panel*) and errors (*right panel*) over the complete WINGS sample. Red-shaded histograms show the overall WINGS redshift distribution, the black histograms show only the distribution of galaxy members.

in 2D). We also separately campare our data with the NOAO Fundamental Plane Survey (NOAO-FPS, Smith et al. 2004), which has a good overlap with our sample, and with the SDSS with which we only have 12 clusters in common. These three comparison samples allow us to compare the data with a uniform (NOAO-FPS and SDSS) and a non-uniform but more extended catalog (NED) in order to check the data quality and also to complete and extend our catalogs with external data.

To make the comparison we selected data in common clusters, cross-correlating the catalogs and taking as common the galaxies whose coordinates differ by less than 6 arcsec. Few galaxies had redshifts that differed by more than 300 km s^{-1}. We checked these galaxies one by one, finding that in all cases the difference arose from a mismatching in the catalogs, so we discarded these objects from the comparison sample. The application of the selection criteria leave us with a final comparison sample of 2218 galaxies. For the 31 clusters in common with the NOAO-FPS, we have a ratio $R = N_{\rm wings}/N_{\rm noao-fps} = 1.73$ of measured redshifts, were $N_{\rm wings}$ is the number of galaxies with redshifts in the WINGS sample and $N_{\rm noao-fps}$ is the number for the NOAO-FPS survey. In particular, this ratio is $R = N_{\rm wings}/N_{\rm noao-fps} = 0.88$ for the northern sample (14 clusters) and $R = N_{\rm wings}/N_{\rm noao-fps} = 2.34$ for the southern sample (16 clusters), emphasizing the different completeness levels in our two

Table 4. Example of data table. The complete redshift catalog is only available in electronic form at the CDS via anonymous ftp to `cdsarc.u-strasbg.fr (130.79.128.5)` or via http://cdsweb.u-strasbg.fr/cgi-bin/qcat?J/A+A/495/707.

Name	R.A. ($J2000$)	Dec ($J2000$)	cz (km s^{-1})	Err (km s^{-1})	r	Memb. Flag	Field
WINGSJ005623.55-005912.6	00:56:23.558	–00:59:12.665	13230	28	11.0	1	A0119
WINGSJ005544.38-005926.6	00:55:44.385	–00:59:26.631	29765	48	4.1	0	A0119
WINGSJ005552.84-005935.7	00:55:52.844	–00:59:35.776	51996	22	6.6	0	A0119
WINGSJ005655.95-005948.2	00:56:55.951	–00:59:48.256	13893	45	5.5	1	A0119
WINGSJ005540.86-005949.5	00:55:40.862	–00:59:49.588	13419	40	5.7	1	A0119
WINGSJ005612.25-010005.2	00:56:12.251	–01:00:05.207	52543	17	9.0	0	A0119
WINGSJ005651.59-010025.7	00:56:51.599	–01:00:25.791	14347	37	6.5	1	A0119
WINGSJ005620.31-010022.6	00:56:20.310	–01:00:22.628	48308	58	2.5	0	A0119
WINGSJ005631.67-010044.9	00:56:31.675	–01:00:44.997	42181	92	4.0	0	A0119
WINGSJ005548.42-010043.1	00:55:48.424	–01:00:43.168	44006	25	5.2	0	A0119
.....	.....	.....	.....	....	....	....	.....

Notes: the columns indicate (1) galaxy names, fiber $J2000$ positions, (2) right ascension (in hours, minutes and seconds), (3) declination (in degrees, arcminutes, arcseconds), (4) heliocentric redshift (in km s^{-1}), (5) error on the redshift measurement (in km s^{-1}), (6) cross-correlation factor, (7) membership flag and (8) cluster field.

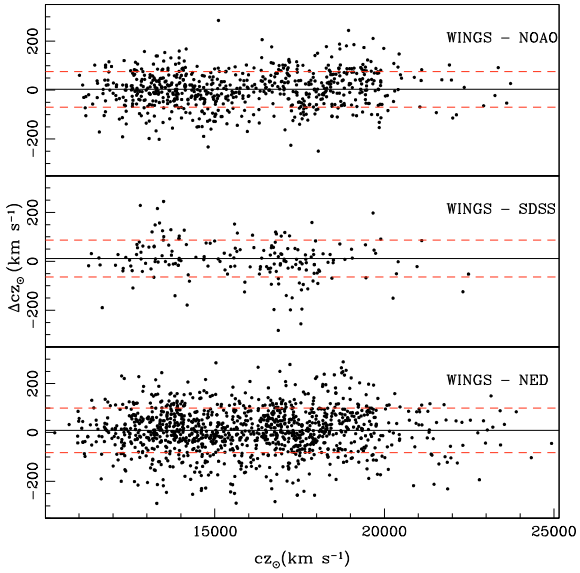

Fig. 4. Plot of the residuals for redshift measurements obtained for the 3 comparison samples used to perform the quality check: NOAO-FPS, SDSS, NED (*from top to bottom*). The black line indicates the offset while the red dashed lines indicate the scatter.

subsamples (north and south). In Fig. 4 we show the global comparison for the 1325 galaxies in common with NED, the 217 in common with SDSS, and 676 in common with NOAO-FPS.

As summarized in Table 5, the mean differences between WINGS and the data in the literature are very low and much lower than the dispersion, assuring the absence of systematic offsets. The different columns refer to: (1) the comparison sample name, (2) mean difference (in km s^{-1}), (3) rms scatter in the differences, and (4) number of galaxies used in the comparison.

Moreover, the dispersion in the measurements is low enough to not greatly influence the measurement of the internal velocity dispersion of galaxy clusters, even in the cases where this quantity is considered low (∼300–400 km s^{-1}) such as for substructures and groups. This fact is fundamental in view of the subsequent dynamical analyses. Particularly discrepant cases can be checked and corrected cluster by cluster.

Table 5. External comparison of redshift.

Sample	Offset km s^{-1}	Scatter km s^{-1}	N
WINGS–NOAO-FPS	3 ± 3	70	676
WINGS–SDSS	11 ± 5	75	217
WINGS–NED	8 ± 3	90	1108

In addition to the three large comparison samples presented above, we have also considered the smaller sample of galaxy clusters presented in the previous work by Bettoni et al. (2006). There are 3 clusters with a total of 23 galaxies in common with this data sample. The mean difference (Δcz) is ∼–9 ± 24 km s^{-1}, while the rms scatter in this case is ∼118 km s^{-1}. The larger scatter is due mainly to the small number statistics.

5.2. Completeness and success rate

It is very important to know the completeness level of the spectroscopic observations as this is a factor that must be accounted for in the derivation of luminosity functions, M/L ratios, as well as any time we want to use the spectroscopic sample to study magnitude-dependent properties (e.g. the different galaxy population fractions inside clusters, see Poggianti et al. 2006). Following the selection criteria described in Sect. 2, the exact cut in the color–magnitude diagram varied slightly from cluster to cluster (in the interval $1.2 \lesssim (B-V)_{5\ \mathrm{kpc}} < 1.4$) due to the small differences in cluster redshift and to minimize the level of contamination from the background. In a few cases, the cut purposely included a secondary red sequence, such as for Abell 151, to also be able to study background clusters. The completeness as a function of magnitude is defined here as:

$$C(m) = \frac{N_z}{N_{\mathrm{ph}}}(m) \tag{3}$$

where N_z is the number of galaxies with measured redshifts and N_{ph} is the number of galaxies in the parent photometric catalog, taking into account the cuts in color and magnitude, for each given magnitude bin m. Completeness is usually a decreasing function of the magnitude because in observations priority

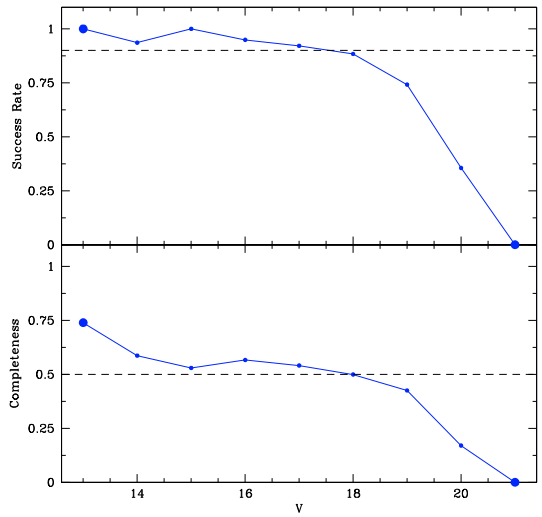

Fig. 5. Success rate (*upper panel*) and global completeness (*lower panel*) for the whole WINGS-SPE sample. Large dots represents bins with low statistic (fewer than 20 points).

is given to brighter objects. The success rate, i.e. the fraction of galaxies with redshift determination with respect to the total number of observed galaxies, is similarly defined as:

$$SR(m) = \frac{N_z}{N_{tg}}(m) \tag{4}$$

where N_z is defined as in Eq. (3) and $N_{\rm tg}$ is the number of target galaxies we actually observed.

The success rate and completeness as a function of V magnitude are shown for the WINGS-SPE sample in Fig. 5. We also computed these two functions separately for the two subsamples observed with the 2dF and WYFFOS spectrographs; they are shown in Fig. 6. We want to emphasise that the quite large difference in the completeness and success rates for the two subsamples is mainly due to two reasons: first, during the observations of the northern sample we lost ∼30% of the observing time due to bad weather conditions. Secondly, the large difference in the number of fibers available (150 with WYFFOS and 400 with AF2) and hence the multiplex power of the two instruments. The effect of the bad weather on the northern sample is particularly evident in the upper panels of Fig. 6. Many galaxies at fainter apparent magnitudes ($V \gtrsim 18$) are lost because of the fact that some faint configurations have spectra with very low S/N and were completely unusable. At variance with this situation, the southern observations show a very flat behavior up to the magnitude limit of the observations ($V \sim 19.5$). Looking at the completeness (lower panels in the figure), the worsening effect due to the bad weather is strengthened by the difference in the number of available fibers that could be placed using the two spectrographs. The almost constant behavior of the completeness for the 2dF observations should to be compared with the resulting monotonically decreasing completeness of the WYFFOS data.

6. Results

6.1. Cluster assignment and redshift histograms

The modelling of galaxy kinematics in clusters remains one of the major tools in determining cluster properties, in particular their mass distribution and dark matter content. Due to projection effects, any cluster kinematic data sample inevitably contains galaxies that are not bound to the cluster and therefore are not good tracers of its gravitational potential. These galaxies are called interlopers. An essential step in dynamical modelling of clusters by any method is therefore to remove such interlopers from the samples or take their presence into account statistically.

The peculiar velocity of a galaxy with redshift z in the rest-frame of a cluster with redshift $z_{\rm cl}$ is given by

$$v = c\frac{z - z_{\rm cl}}{1 + z_{\rm cl}} \tag{5}$$

valid to first-order for $v \ll c$ (e.g. Harrison 1974; Carlberg et al. 1996). The dispersion of the v values for the cluster members define the cluster rest-frame velocity dispersion $\sigma_{\rm cl}$ that is related to the observed velocity dispersion:

$$\sigma_{\rm cl} = \frac{\sigma_{\rm obs}}{1 + z_{\rm cl}} \cdot \tag{6}$$

It is very important to determine as accurately as possible which galaxies belong to the clusters and which ones have to be considered as interlopers, and thus removed. It is known that the presence of interlopers can increase the value of the observed velocity dispersion and since the estimated virial mass is proportional to the third power of this value, a small error in the velocity dispersion can highly influence the mass estimate. We employ an iterative $\pm 3\sigma$ clipping scheme to determine which galaxies are cluster members (Yahil & Vidal 1977). This works as follows.

A first estimate of $z_{\rm cl}$ is obtained from a visual inspection of the redshift histogram, usually corresponding to the statistical mode for the given distribution. Galaxies with redshifts outside the region $z_{\rm cl} \pm 0.015$ (corresponding to ∼4000 km s^{-1}) are removed and not used in any further analysis. The following two steps are then iterated until convergence on $z_{\rm cl}$ and $\sigma_{\rm cl}$ is reached: (1) calculate v for all the galaxies using Eq. (5); (2) for galaxies with v in the interval $[-3\sigma_{\rm cl},+3\sigma_{\rm cl}]$, a new estimate of $z_{\rm cl}$ and $\sigma_{\rm cl}$ is calculated using the robust biweight location and scale estimators (Beers et al. 1990).

This approach is still widely used today (e.g., see Milvang-Jensen et al. 2008) even if different methods of interloper removal based on dynamical or statistical restrictions imposed on ranges of positions and velocities available to cluster members have been developed. We have decided to use this method because, despite its intrinsic simplicity, it has been demonstrated to be the most effective to determine cluster membership in many cases (e.g., Wojtak et al. 2007). Since in this paper we are only interested in the global value of the cluster velocity dispersions, we do not need here to investigate different methods of interloper removal, as the values of the cluster velocity dispersions would only marginally be modified. We will perform a more detailed analysis of the dynamics of the WINGS galaxy clusters in a following paper (Cava et al. 2009, in prep.), where more sophisticated methods of interloper removal will also be exploited.

Our velocity dispersions are not all evaluated at the cluster virial radius, since our observations do not always go that far. Cluster velocity dispersions are known to depend on radius, hence on the aperture used to measure them (Fadda et al. 1996; Rines & Diaferio 2006; Muriel et al. 2002; Girardi & Mezzetti 2001; Aguerri et al. 2007). However, the dependence is very mild for galaxy clusters in the range of apertures considered here, i.e. $(\sim 0.8 \pm 0.2) \times R_{200}$, and is probably

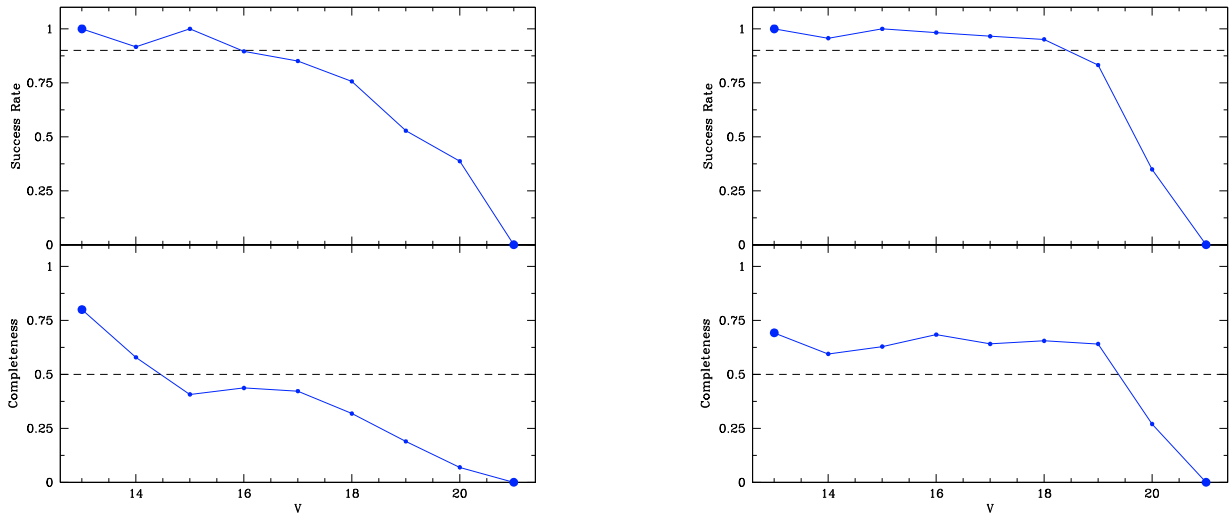

Fig. 6. Success rate and global completeness for WYFFOS (*left plot*) and 2dF observations (*right plot*). Large dots represents bins with low statistic (fewer than 10 points).

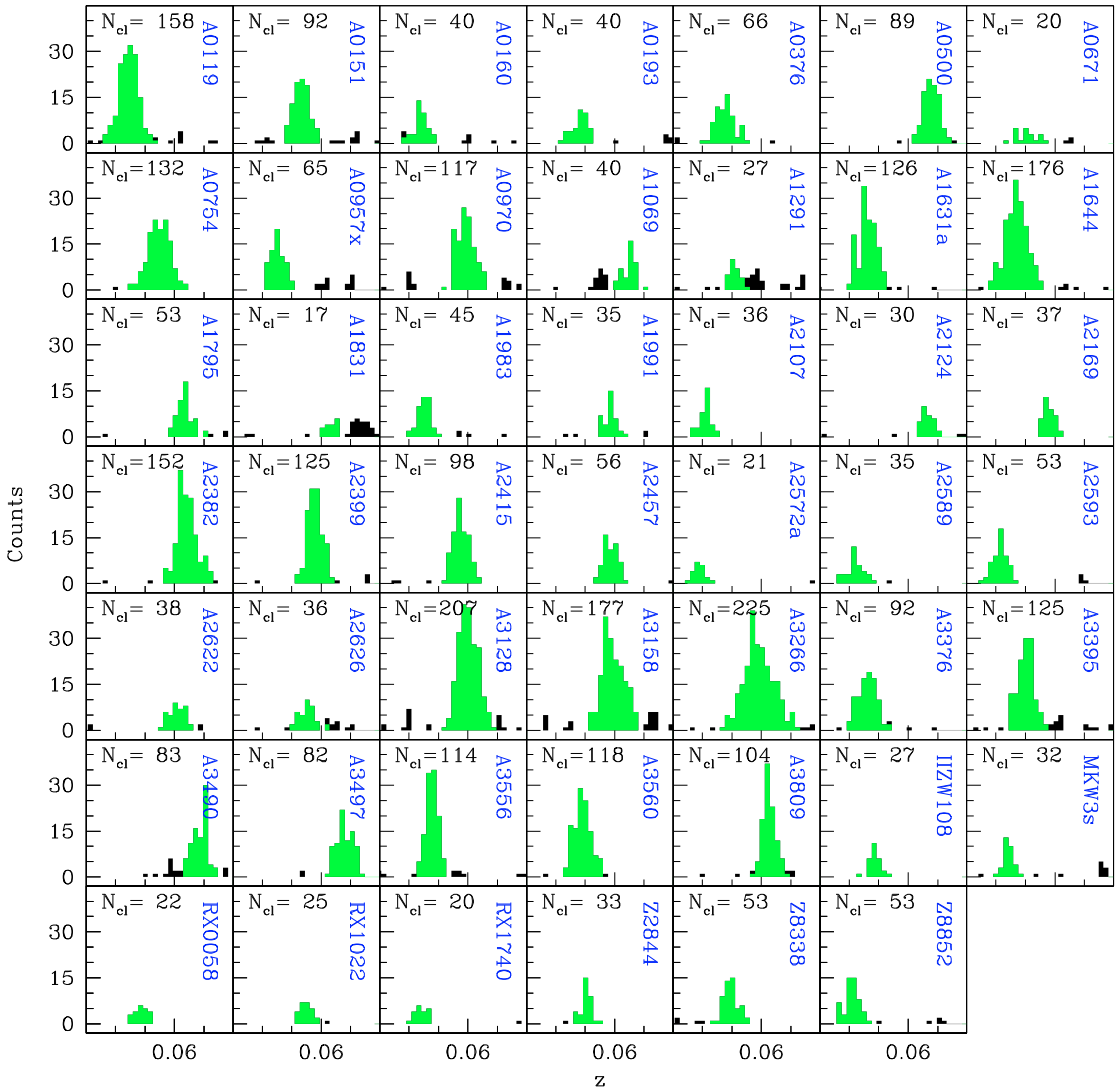

Fig. 7. Histograms of the WINGS-SPE data sample in the range $0.03 \leq z \leq 0.08$. In color are histograms for cluster members defined using a 3σ cut. $N_{\rm cl}$ indicates the number of cluster galaxies inside 3σ from the mean cluster redshift.

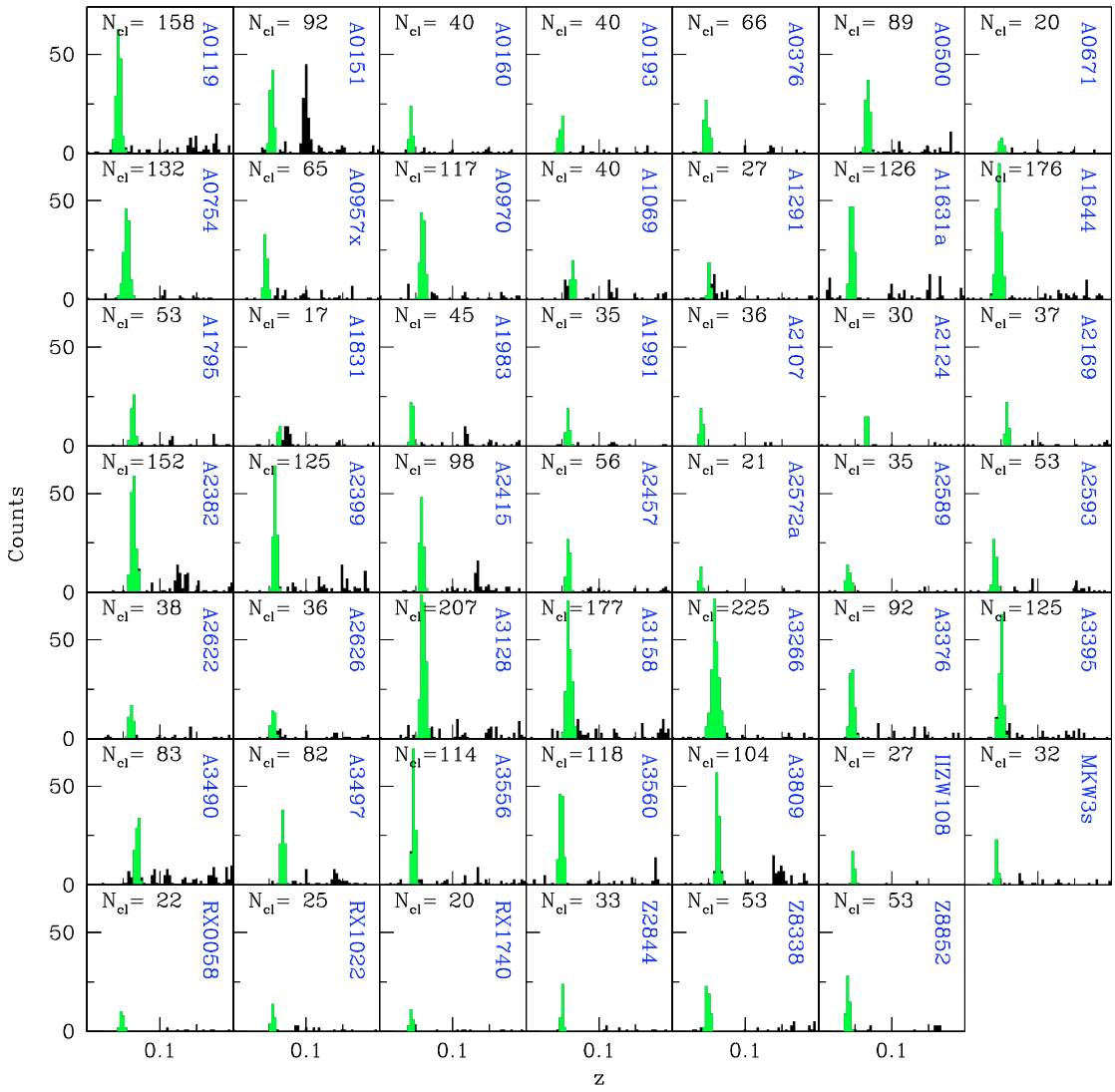

Fig. 8. Histograms of the WINGS-SPE data sample in the wide-range $0 \leq z \leq 0.2$ where fore/background objects are visible. In green are histograms for cluster members defined using a 3σ cut. N_{cl} indicates the number of cluster galaxies inside 3σ from the mean cluster redshift.

smaller than 10%, as demonstrated for example by the analysis of Łokas & Mamon 2001 (see their Fig. 7) or as shown by Aguerri et al. (2007) for a large sample of nearby clusters (they find a variation lower than 3% recomputing the velocity dispersions inside apertures of $0.4 \times R_{200}$ and $0.6 \times R_{200}$). In Cols. 11 and 12 of Table 1 we report the virial radius in Mpc and the maximum observed aperture radius in unit of R_{200} for each cluster, that is the maximum dynamical radius for which we have spectroscopic data. From Table 1 it can also be seen that ~40% of the observed clusters achieve an aperture radius $\gtrsim 0.9 \times R_{200}$.

Velocity dispersions estimates, σ_W (in km s^{-1}), for the WINGS-SPE sample are listed in Col. 7 of Table 1. The errors quoted here were obtained using the classical jackknife technique (Efron 1982). For comparison, values of σ found in the literature (σ_L) are given in Col. 8.

In Fig. 7, we show the observed redshift histograms of clusters in the WINGS-SPE sample. In each panel the redshift distributions for the galaxies assigned to the cluster are plotted in green. The bin size in redshift is 0.0015. A hint of the presence of substructures in some clusters can already be seen here. The same plot but for a larger redshift range ($0 \leq z \leq 0.2$) is given in Fig. 8; the foreground and background galaxies are much more evident here. In some cases a secondary peak indicating a background or a foreground cluster can be seen as well, such as in the case of *A*0151, *A*1631*a*, and *A*2382. In these cases the bin size is larger and equal to 0.004.

In Fig. 9 we present velocity diagrams for each cluster. Cases where there are additional sub-structures around the main cluster are even more evident in these plots. Green points indicate galaxies assigned as cluster members using the procedure explained above. Also indicated in each plot is the value of R_{200} (in Mpc), the radius inside which the mean density of the cluster is 200 times the critical density of the universe, and the value of the cluster velocity dispersion, σ_{cl} (in km s^{-1}). R_{200} was computed from σ_{cl} as in Poggianti et al. (2006):

$$R_{200} = 1.73 \frac{\sigma_{cl}}{1000 \text{ km s}^{-1}} \frac{1}{\sqrt{\Omega_\Lambda + \Omega_0 (1 + z_{cl})^3}} h^{-1} \text{ Mpc} \qquad (7)$$

with $\Omega_\Lambda = 0.7$, $\Omega_0 = 0.3$, $h = 0.7$.

With these new data, the mean of the ratio of the number of galaxies we used to derive the cluster velocity dispersion to the numbers that were used for the literature values is $R = N_{wings}/N_{tab} = 2.71$. Hence our measurements are based on almost three times as many member galaxies in comparison to previous measurements. The spectroscopic velocity dispersions for the WINGS-SPE sample are in the range 400 to 1300 km s^{-1},

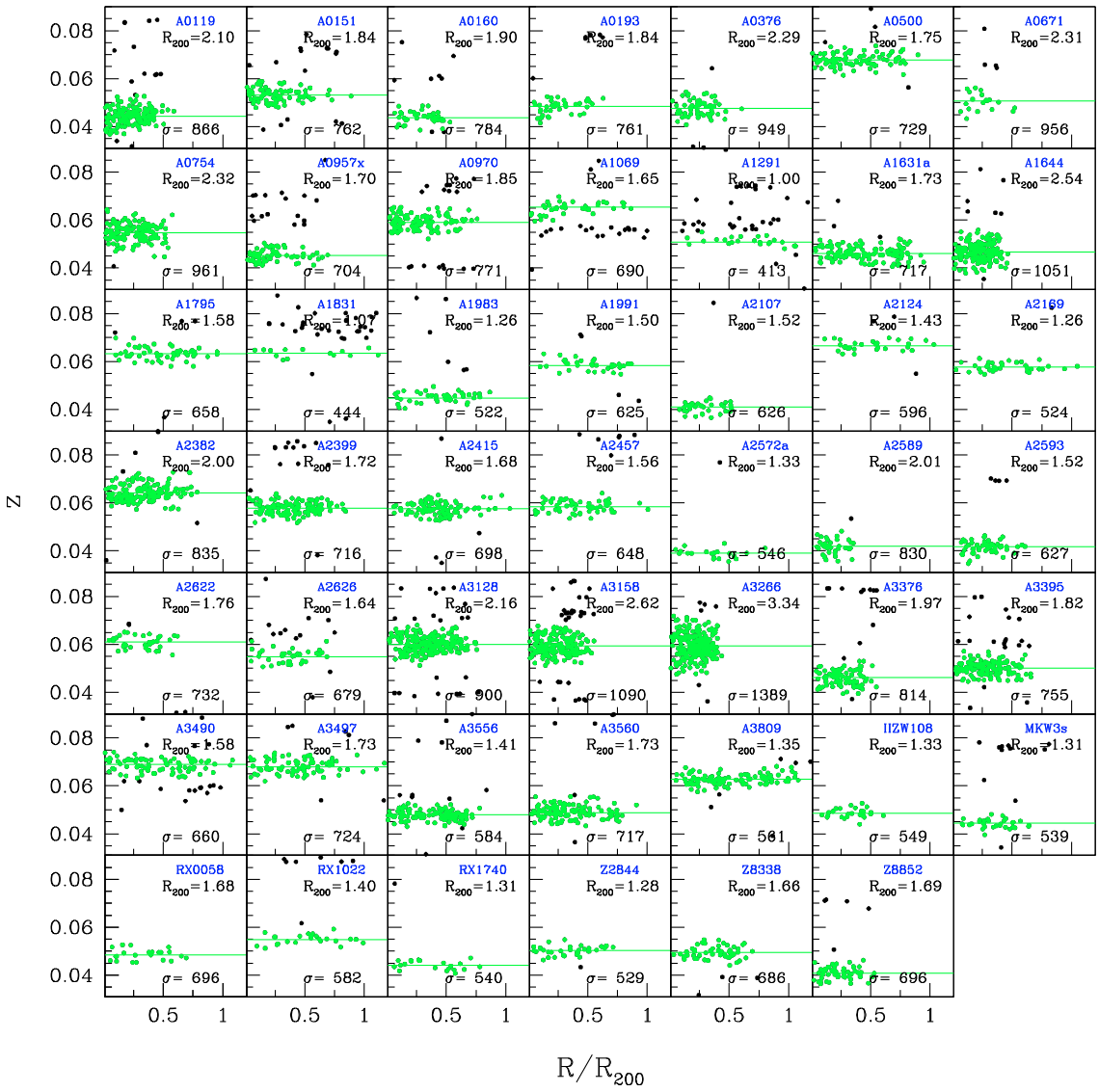

Fig. 9. Velocity diagrams of the WINGS-SPE data sample in the range $0.03 \leq z \leq 0.09$ as a function of the normalized radius (R/R_{200}). Green points indicate cluster members, the horizontal line is the mean redshift. R_{200} and σ are also indicated in each box.

and are generally higher than the velocity dispersions for the SDSS sample at similar redshift (Miller et al. 2005).

6.2. X-ray luminosity-velocity dispersion relation

In this section we evaluate the strength and shape of the correlation between X-ray luminosity and velocity dispersion for our sample of clusters. Self-similar models assume that the dominant energy source in the cluster comes from the gravitational collapse, predicting scaling relations of the form: $L_x \propto T^2 \propto \sigma_v^4$. While there seems to be general agreement between different measurements that $L_x \propto T^{\sim 3}$, the measurement of $L_x - \sigma_v$ has so far given contradictory results. Some authors have found that $L_x \propto \sigma^4$ (although with quite large measurement errors because of rather small data samples), while others find slopes larger than 4 (see e.g. Xue & Wu 2000; Ortiz-Gil et al. 2004). Some of the differences in the results could arise from the different ways the samples are selected, with a preference for more regular clusters in some of these surveys. It has also been suggested that clusters and groups do not follow the same $L_x - \sigma_v$ scaling relation, the latter being flatter than the former (e.g. Mahdavi et al. 2000; Xue & Wu 2000). However, there are other measurements that contradict that conclusion (e.g. Mulchaey & Zabludoff 1998; Mahdavi & Geller 2001). For more distant clusters (z between ~0.15 and ~0.6) there is some evidence that the slope is also >4 (Borgani et al. 1999b; Girardi & Mezzetti 2001), although only small samples are available at the moment, and more data are needed to reduce the error bars.

In Fig. 10, the X-ray luminosities, L_x of the clusters in our WINGS-SPE sample are plotted against their velocity dispersion, σ_W, with the best fit relation shown. σ_W is from our measurements and the X-ray luminosities are taken from Ebeling et al. (1996) and are in the 0.1–2.4 keV ROSAT RASS bandpass (see Cols. (7) and (10) of Table 1 respectively). The marginal distributions of the X-ray luminosities and velocity dispersions are shown in the side panels. Performing an orthogonal fit, the best fit relation is given by:

$$\log(L_x) = (32.6 \pm 1.7) + (4.0 \pm 0.3) \times \log(\sigma_v) \quad (8)$$

with L_x in units of erg s^{-1} and σ_v in km s^{-1}. The observed slope of 4.0 ± 0.3 is in good agreement with the value measured by Mulchaey & Zabludoff (1998), Mahdavi & Geller (2001), Girardi & Mezzetti (2001) and Ortiz-Gil et al. (2004). For the intercept, the result is compatible with Mahdavi & Geller (2001),

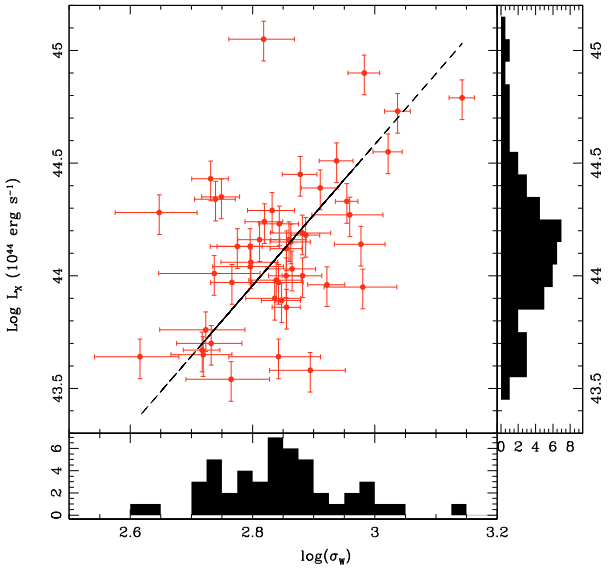

Fig. 10. X-ray luminosity versus velocity dispersion σ_v relation for the 48 clusters in the WINGS sample. The marginal distributions are also shown.

Girardi & Mezzetti (2001) and Ortiz-Gil et al. (2004) at about one-sigma confidence level.

7. Summary

As part of the WINGS-SPE survey, we have carried out spectroscopic observations of galaxies in 48 clusters using the WHT/AF2 and AAT/2dF facilities. These observations have yielded redshifts for 6137 galaxies, which have been used to derive precise redshifts and velocity dispersions for our clusters. By combining these data with those already available in the literature, we now have velocity dispersions for all the clusters in the WINGS sample.

In Table 4 we present the complete and final set of redshift data now available for the WINGS galaxy clusters. A total of 3647 galaxies turn out to be members of our clusters, thereby almost doubling the number of known members in this sample of nearby clusters. We have shown that our reduction and measurement procedures result in high quality redshift measurements. A comparison with data available in the literature to both check the accuracy and consistency of our measurements and to increase our overall redshift sample has been done. Using an iterative 3σ clipping scheme, we have derived velocity dispersions for all the 48 WINGS-SPE clusters. The mean of the ratio of the number of galaxies we used to derive the cluster velocity dispersion and the number that were used for the literature values is $R = N_{\rm wings}/N_{\rm tab} = 2.71$. This means that our velocity dispersion values are based on almost three times as many member galaxies than previous measurements. We found that the X-ray luminosity – velocity dispersion (L_x–σ) relation for our sample of 48 clusters has $L_x \propto \sigma^4$, although with a large scatter. Finally, we note that the WINGS clusters have a wide range of velocity dispersion values. The implied large range of masses therefore makes the WINGS cluster sample an unprecedented and unique dataset to study the processes affecting cluster galaxy evolution as a function of cluster mass. Future papers in this series will exploit this data set to perform a dynamical analysis of the WINGS sample of galaxy clusters and a substructure analysis.

Acknowledgements. We wish to thank the anonymous referee for useful comments that have improved this manuscript.

References

Aguerri, J. A. L., Sánchez-Janssen, R., & Muñoz-Tuñon, C. 2007, A&A, 571, 17
Bahcall, N. A., McKay, T. A., Annis, J., et al. 2003, ApJS, 148, 243
Beers, T. C., Flynn, C., & Gebhardt, K. 1990, AJ, 100, 32
Bettoni, D., Moles, M., Kjærgaard, P., et al. 2006, A&A, 452, 811
Bird, C. M. 1994, AJ, 107, 1637
Biviano, A., Katgert, P., Thomas, T., et al. 2002, A&A, 387, 8
Borgani, S., Girardi, M., Carlberg, R. G., et al. 1999a, ApJ, 527, 561
Borgani, S., Rosati, P., Tozzi, P., et al. 1999b, ApJ, 517, 40
Burgett, W. S., Vick, M. M., Davis, D. S., et al. 2004, MNRAS, 352, 605
Carlberg, R. G., Yee, H. K. C., Ellingson, E., et al. 1996, ApJ, 462,32
Dekel, A. 1994, ARA&A, 32, 371
De Propris, R., Couch, W. J., Colless, M., et al. 2002, MNRAS, 329, 87
Dressler, A. 1980, ApJS, 42, 565
Dressler, A., & Shectman, S. A. 1988, AJ, 95, 985
Dressler, A., Lynden-Bell, D., Burstein, D., et al. 1987, ApJ, 313, 42
Dressler, A, Oemler, A. J., Couch, W. J., et al. 1997, ApJ, 490, 577
Ebeling, H., Voges, W., Bohringer, H., et al. 1996, MNRAS, 281, 799E
Ebeling, H., Edge, A. C., Bohringer, H., et al. 1998, MNRAS, 301, 881
Ebeling, H., Edge, A. C., Allen, S. W., et al. 2000, MNRAS, 318, 333
Edge, A. C., & Stewart, G. C. 1991, MNRAS, 252, 414
Efron, B. 1982, The Jackknife, the Bootstrap and Other Resampling Plans, Philadelphia: SIAM
Escalera, E., Biviano, A., Girardi, M., et al. 1994, ApJ, 423, 539
Fadda, D., Girardi, M., Giuricin, G., et al. 1996, ApJ, 473, 670
Fasano, G., Poggianti, B. M., Couch, W. J., et al. 2000, ApJ, 542, 673
Fasano, G., Marmo, C., Varela, J., et al. 2006 A&A, 445, 805
Fisher, D., Fabricant, D., Franx, M., et al. 1998, ApJ, 498, 195
Flin, P., & Krywult, J. 2006, A&A, 450, 9
Fritz, J., Poggianti, B.M., Bettoni, D., et al. 2007, A&A, 470, 137
Girardi, M., & Mezzetti, M. 2001, ApJ, 548, 79
Girardi, M., Fadda, D., Giuricin, G., et al. 1996, ApJ, 457, 61
Girardi, M., Escalera, E., Fadda, D., et al. 1997, ApJ, 482, 41
Goto, T., Sekiguchi, M., Nichol, R. C., et al. 2002, AJ, 123, 1807
Harrison, E. R. 1974, ApJ, 191, L51
Jacoby, G. H., Hunter, D. A., & Christian, C. A. 1984, ApJS, 56, 257
Kurtz, M. J., & Mink, D. J. 1998, PASP, 110, 934
Lewis, I. J., Cannon, R. D., Taylor, K., et al. 2002, MNRAS, 333, 279
Łokas, E. L., & Mamon, G. A. 2001, MNRAS, 321, 155
Lubin, L. M., Oke, J. B., & Postman, M. 2002, AJ, 124, 1905
Lynden-Bell, D., Faber, S. M., Burstein, D., et al. 1988, ApJ, 326, 19
Mahdavi, A., & Geller, M. J. 2001, ApJ, 554, L129
Mahdavi, A., Bohringer, H., Geller, M. J., et al. 2000, ApJ, 534, 114
Mazure, A., Katgert, P., den Hartog, R., et al. 1996, A&A, 310, 31
Miller, C. J., Nihcol, R. C., Reichart, D., et al. 2005, AJ, 130, 968
Milvang-Jensen, B., Noll, S., Halliday, C., et al. 2008, A&A, 482, 419
Mulchaey, J. S., & Zabludoff, A. I. 1998, ApJ, 496, 73
Muriel, H., Quintana, H., Infante, L., et al. 2002, AJ, 124, 1934
Ortiz-Gil, A., Guzzo, L., Schuecker, P., et al. 2004, MNRAS, 348, 325
Poggianti, B. M., von der Linden, A., De Lucia, G., et al. 2006, ApJ, 642, 188
Postman, M., Franx, M., Cross, N. J. G., et al. 2005, ApJ, 623, 721
Quintana, H., & Melnick, J. 1982, AJ. 87, 972
Ramella, M., Biviano, A., Pisani, A., et al. 2007, A&A, 470,39
Rhee, G. F. R. N., van Haarlem, M. P., & Katgert, P. 1991, A&A, 246, 301
Rines, K., & Diaferio, A. 2006, AJ, 132, 1275
Smith, R. J., Hudson, M. J., Nelan, J. E., et al. 2004, AJ, 128, 1558
Solanes, J. M., Salvador-Solé, E., & González-Casado, G. 1999, A&A, 343, 733
Strauss, M. A., & Willick, J. A. 1995, Phys. Rep., 261, 271
Struble, M. F., & Ftaclas, C. 1994, AJ, 108, 1
Struble, M. F., & Rood, H. J. 1999, ApJ, 125, 35
Taylor, K., Bailey, J. A., Wilkins, T., et al. 1996, in Astronomical Data Analysis and Systems V, ed. G. H. Jacoby, J. Barnes, ASP Conf. Ser. 101, Astron. Soc. Pac., San Francisco, 195
Tonry, J. L., & Davis, M. 1981, ApJ, 246, 666
Tran, K. H., Kelson, D. D., van Dokkum, P., et al. 1999, ApJ, 522, 39
Varela, J., D'Onofrio, M., Marmo, C., et al. 2009, A&A [arXiv:0902.0612]
West, M. J., & Bothun, G. D. 1990, ApJ, 350, 36
West, M. J., Jones, C., & Forman, W. 1995, ApJ, 451, L5
Wojtak, R., Łokas, E. L., Mamon, G. A., et al. 2007, A&A, 466, 437
Wu, X.-P., Fang, L.-Z., & Xu, W. 1998, A&A, 338, 813
Xue, Y., & Wu, X.-P. 2000, ApJ, 538, 65
Yahil, A., & Vidal, N. V. 1977, ApJ, 214, 347